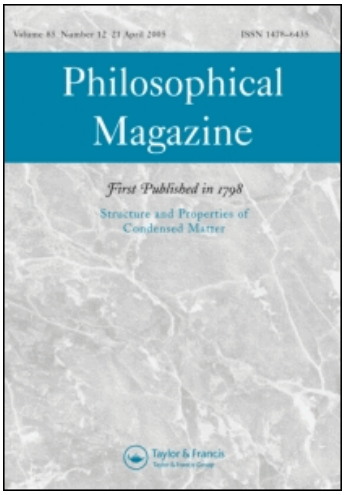

Philosophical Magazine
Publication details, including instructions for authors and subscription information:
http://www.informaworld.com/smpp/title~content=t713695589

Size effects in yield and plasticity under uniaxial and non-uniform loading: Experiment and theory

A. J. Bushby[a]; D. J. Dunstan[b]
[a] Department of Materials, Centre for Materials Research, Queen Mary University of London, London, E1 4NS, UK [b] Department of Physics, Centre for Materials Research, Queen Mary University of London, London, E1 4NS, UK

First published on: 02 July 2010

To cite this Article Bushby, A. J. and Dunstan, D. J.(2010) 'Size effects in yield and plasticity under uniaxial and non-uniform loading: Experiment and theory', Philosophical Magazine,, First published on: 02 July 2010 (iFirst)
To link to this Article: DOI: 10.1080/14786435.2010.493533
URL: http://dx.doi.org/10.1080/14786435.2010.493533

Philosophical Magazine
2010, 1–13, iFirst

Taylor & Francis
Taylor & Francis Group

Size effects in yield and plasticity under uniaxial and non-uniform loading: Experiment and theory

A.J. Bushby[a] and D.J. Dunstan[b]*

[a]*Department of Materials, Centre for Materials Research, Queen Mary University of London, London, E1 4NS, UK;* [b]*Department of Physics, Centre for Materials Research, Queen Mary University of London, London, E1 4NS, UK*

(*Received 11 November 2009; final version received 12 May 2010*)

The size of microstructural features has long been known to determine the strength of materials, as in the Hall–Petch effect of grain size. More recently, the importance of the size of the structure itself (thin foil, wire or pillar) or of the loaded volume (indentation) has been recognised. Many phenomenological theories have been proposed to account for the size effect. Here, experimental data of very high accuracy are reported on copper wire in torsion which distinguish the size effects of grain size and structure size on the elastic limit and on the flow stress at low plastic strain. The data are compared with less accurate data from similar wires in tension. The size effects are shown to arise by first-principles analysis of dislocation behaviour, exploiting the slip-distance theory of Conrad together with forest (Taylor) work-hardening theory, but with modifications to both theories to account for finite structure size. The resulting theory is compatible with the concepts of dislocation starvation and of strain-gradient plasticity. The size effect in the elastic limit is due to the constraint the size puts on dislocation curvature, while the size effect on the flow stress is due to the constraint size puts on dislocation mean free path and to the fate of a dislocation after it has moved.

Keywords: strengthening mechanisms; plasticity; size effect; stress–strain measurement; copper wire; torsion; tensile testing

1. Introduction

In the early 1950s, Hall [1] and Petch [2] reported that the strength of a polycrystalline metal varies as the inverse square-root of the grain size. Despite the accumulation of a massive experimental database and several theories of the effect, no single secure theoretical explanation of this behaviour has been established. More recently, the increase in strength of metals and ceramics in the presence of a large strain gradient, or when only a small volume of material is stressed, has become well established [3–9]. However, the experimental data has lacked the precision to pin down the circumstances and the reasons for this. Effects of size on strain-hardening and on initial plastic yield have been difficult to distinguish, especially in soft metals where the experimental data has not been able to identify a clear elastic

*Corresponding author. Email: d.dunstan@qmul.ac.uk

ISSN 1478–6435 print/ISSN 1478–6443 online

DOI: 10.1080/14786435.2010.493533
http://www.informaworld.com

limit or yield point. It has always been possible to consider that a putative yield stress σ_Y is really only the flow stress $\sigma(\varepsilon_{pl})$ at the smallest plastic strain ε_{pl} which is experimentally resolvable. Consequently, it has always remained possible to explain the observed size effects in terms of work-hardening effects or dislocation–dislocation interaction models. On the other hand, the epitaxial growth of strained semiconductor layers has shown unambiguously that the primary size effect is in the yield point and the key concept is whether a single dislocation is energetically favoured. This is fully developed in the theory of critical thickness, due to Frank and van der Merwe [10] and Matthews [11], and reviewed by Fitzgerald [12] and Dunstan [13]. Recent experiments on indentation of strong metals and ceramics have suggested that the size effects operate both at the elastic limit and through the strain-hardening [6,14].

In two classic papers in the 1990s, Fleck et al. [3] and Stölken and Evans [4] reported size effects in small metal structures at large strains and interpreted their results using strain-gradient plasticity theory (SGP), in which the plastic strain gradient in these experiments causes the increased strength through the mechanism of the geometrically necessary dislocations, which are the microscopic manifestations of a plastic strain gradient. This theory says nothing about grain size. However, we reported nanoindentation experiments using spherical indenters with a range of radii on specimens with a range of grain sizes [14] (small indenter radius necessarily induces larger strain gradients than larger indenter radius). We found that the indenter size and the grain size interact in determining the observed hardness. Finding that the interaction is of the form:

$$\frac{1}{\ell_{\text{eff}}} = \frac{1}{h} + \frac{1}{d}, \tag{1}$$

where h is the indentation contact size and d is the average grain size (for single crystal specimens, d may reasonably be set to infinity), with the observed hardness varying as the inverse square root of ℓ_{eff}, we surveyed other data to test this formulation [15]. Copper bulge-test data from Xiang et al. [16], nickel foil bending data from Ehrler et al. [17], copper indentation data from Hou et al. [14] and simulated wedge indentation data for polycrystalline material using discrete dislocation dynamics modelling reported by Widjaja et al. [18] were all fitted to this expression. It was found to be quite generally applicable to the size effects in these data.

Nanoindentation and the other works cited do not adequately distinguish between the behaviour at the elastic limit (yield point) and the behaviour at some proof strain or flow stress. Foil-bending experiments can detect elastic behaviour and plastic behaviour, but do not have very high resolution in the transition region around the yield point. Strained semiconductor epitaxial thin films are the simplest system in which to study the onset and evolution of plastic yield. Even there, however, it was difficult to distinguish and understand the conditions for plastic yield through the movement of existing dislocations, described by the Matthews thermodynamic critical thickness theory, and the conditions for gross plastic yield through the activation of dislocation multiplication mechanisms, until the experimental work of Whitehouse et al. [19] and Dixon and Goodhew [20] and the theoretical work of Beanland [21] made this distinction clear [13]. Wire-torsion

experiments are capable of very high resolution in the low-strain region. In this paper, therefore, we report high-resolution wire-torsion experiments on thin copper wires in Section 2, in which we can distinguish the size effect on the elastic limit (when the first irreversible dislocation motion takes place) from the size effect on the gross plastic yield point when dislocation sources are activated throughout the specimen. In Section 3, we show that the data are compatible with a modified slip-distance theory which accounts separately for a size effect on the elastic limit (yield point) and on the flow stress during plastic deformation. A preliminary account of this work has been given in Dunstan et al. [22].

Experiments under tension are much less sensitive, but we present preliminary data showing that at small plastic strains the theoretical fit for torsion accounts for the tensile data. At higher strains the tensile data deviates. The implications and the application of the theory to other experimental situations are discussed in Section 4.

2. Experiment and results

Copper wires of diameters 10 μm (from Goodfellows, purity 99.99%) and 50 μm (from Comax, purity 99.99% spec C101) were wound on a bobbin and annealed in a rapid thermal annealing furnace (600–700°C, 10–150 s) to give a range of grain sizes. Three wires were taken through all steps of the torsion experiment successfully, one of 10 μm diameter and two of 50 μm diameter, while tensile data was obtained from two 10 μm and one 50 μm diameter wires. Grain sizes were measured by focussed ion-beam (FIB) microscopy, using the strong channelling contrast associated with the secondary electrons emitted. The numbers of grains along a line of specified length were counted on images of the cylindrical surface of the wire or on images of flat cross-sections made by FIB milling (Figure 1). We do not consider that the grain sizes are highly accurate but they are certainly representative.

Lengths of wire up to 1 m long were then suspended vertically and a small crossbar was fixed at the bottom. The crossbar assembly weighed 18 mg for the 50 μm wires and 6 mg for the 10 μm wire, giving tensile stresses of 0.09 and 0.75 MPa, respectively, well below the elastic limit shear stresses of about 20 and 50 MPa, respectively, observed experimentally (see below). To anneal out any strain-hardening due to unwinding the wires from the bobbins and other handling, electrical contacts were made at the top and bottom, and, in a nitrogen ambient, an electrical current of 1.1 A (50 μm wires) and 0.17 A (10 μm wires) was passed for 150 s. This heated the wires to about 300–400°C (estimated both from the thermal expansion of the wires and from their increase in resistance).

A turntable with a pair of pins engaging with the crossbar (Figure 2) was used to twist the wires to various twist angles φ_L (radians), the 'Load' condition, which corresponds to surface shear strains of

$$\theta_S = \frac{a}{L}\varphi_L, \tag{2}$$

where a is the radius of the wire and L is the gauge length. After each successive value of φ_L, the turntable was backed off until the wire hung freely, when the unload angle,

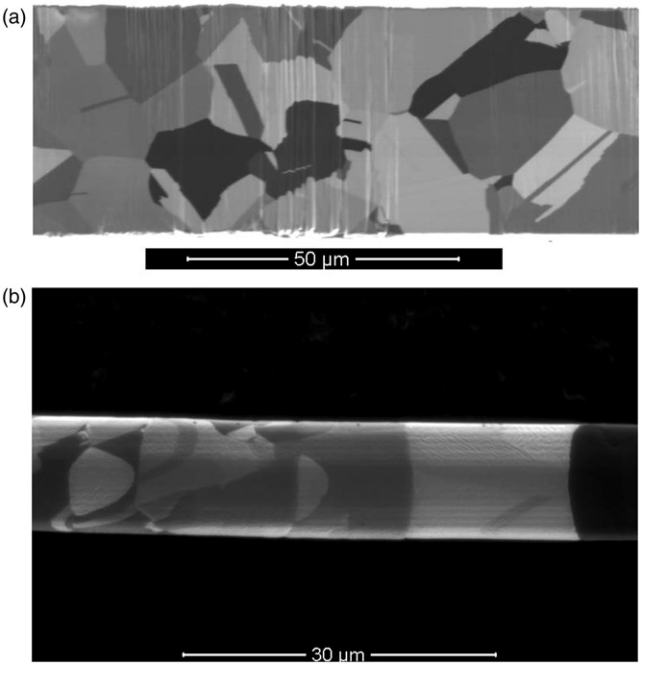

Figure 1. Focussed ion beam secondary electron images of (a) FIB cross-sectioned 50 μm diameter wire, showing the grain structure and the measured grain size is 10.0 μm, and (b) surface image of the 10 μm diameter wire, showing the grain structure and the measured grain size is 9.7 μm.

φ_U, was measured. With the crossbar and pins in air, apparently random motions of the crossbar, driven perhaps by draughts or electrostatic forces, limited the accuracy. This was the set-up used for the 10 μm wire and one of the 50 μm wires. The experiment was then improved by immersing the crossbar and pins in water, held in a beaker which revolved with the turntable. A second stationary beaker inside this one acted as a stator to reduce rotation of the water at the crossbar. A small video camera was introduced to view the crossbar and pins from directly underneath. Under these conditions, the angles of the crossbar in the 'Unload' condition, φ_U (the untwist angle), could be measured to an accuracy of about 3° or 0.05 radians. The unload angles are a direct measure of the plastic torsion of the wire:

$$\theta_{pl} = \frac{a}{L}\varphi_U. \tag{3}$$

The difference between the twist ('Load') and untwist ('Unload') angles is a direct measure of the torque in the 'Load' condition:

$$Q = \frac{G\pi a^4}{2L}(\varphi_L - \varphi_U) \quad Q_n = \frac{Q}{a^3}, \tag{4}$$

where G is the shear modulus. We do not use the torque in what follows, preferring to calculate the twist and untwist angles directly. However, the normalised torque Q_n

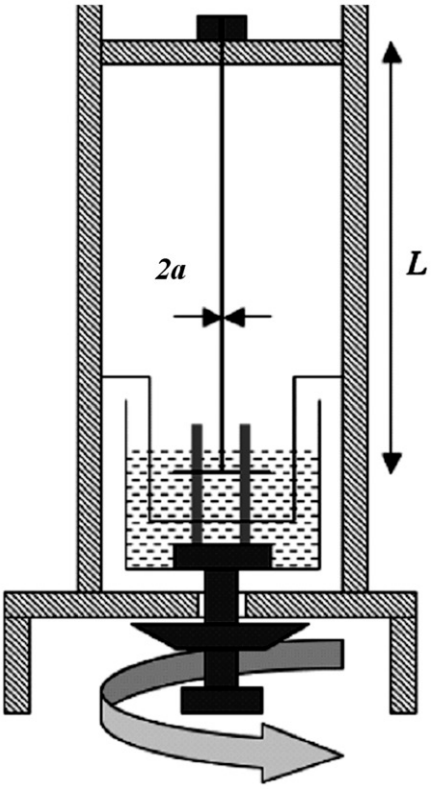

Figure 2. Apparatus for the torsion experiments is shown schematically.

has units of Pa and it is representative of the stress – in the fully elastic case it is proportional to the surface stress – so the load–unload experiment obtains a representation of the stress–strain curve. Figure 3 shows the data around the elastic limit up to very small plastic strain, plotted in the form φ_U against φ_L to make clear the elastic region $\varphi_U = 0$ and the breakpoint at the elastic limit to the plastic regime $\varphi_U > 0$. In Figure 4, the data for much higher strains is shown in a more conventional form, plotting $\varphi_L - \varphi_U$ against φ_L since this is analogous to the stress–strain curve.

Using the same apparatus as for wire twisting, so that wires could again be annealed *in situ* after handling, wires were also loaded in tension by applying and removing small masses in the form of hooked wires hung on the crossbar. A device for lowering and raising the masses onto the crossbar was used to avoid rough handling of the wire. The masses were weighed on a chemical balance to the nearest milligram and the displacements were measured using a travelling microscope to about $\pm 5\,\mu$m. The engineering stress and strain were determined as

$$\sigma = \frac{mg}{\pi a^2} \quad \varepsilon = \frac{\Delta L}{L}. \tag{5}$$

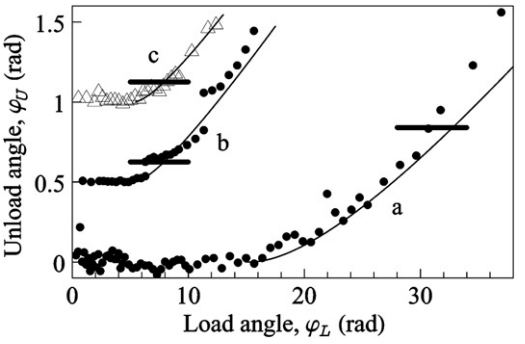

Figure 3. Torsion data around the elastic limit are plotted for (a) the 10 μm diameter wire with $d = 11$ μm, length $L = 26$ cm, (b) the 50 μm wire with $d = 8$ μm and $L = 97$ cm, and (c) the 50 μm wire with $d = 21$ μm and $L = 97$ cm; (b) and (c) are offset by 0.5 and 1 radian for clarity. The dataset (b) was measured under water as described in the text. The two jumps in this dataset are due to creep during a 10 min pause under load at two values of φ_L. The solid curves are fits for $\varphi_L > \varphi_{LS}$ as described in the text. The heavy horizontal lines show the unload angle due to the plastic strain corresponding to a single axial screw dislocation. One radian corresponds to a surface strain of 1.9×10^{-5} for the 10 μm wire and 2.6×10^{-5} for the 50 μm wire.

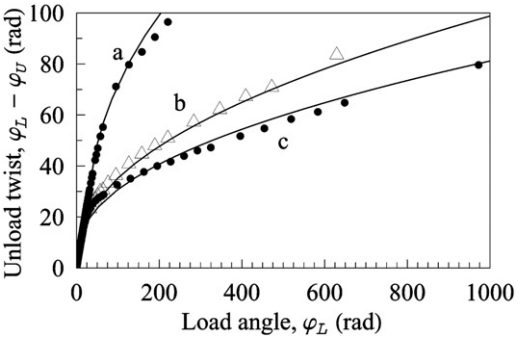

Figure 4. Torsion data at higher strain are plotted for (a) the 10 μm diameter wire with $d = 11$ μm, length $L = 26$ cm, (b) the 50 μm wire with $d = 8$ μm and $L = 97$ cm, and (c) the 50 μm wire with $d = 21$ μm and $L = 97$ cm. The solid lines are fits for $\varphi_L > \varphi_{L0}$ as described in the text. 100 radians corresponds to a surface strain of 0.0019 for the 10 μm wire and 0.0026 for the 50 μm wire.

Three wires were measured successfully, two of 10 μm diameter and one of 50 μm diameter. The data is shown in Figure 5.

3. Theory and fit to data

Conrad's slip-distance theory [23] begins with the definition of plastic strain (here, shear plastic strain):

$$\varepsilon_{pl} = b\bar{x}\rho_m, \tag{6}$$

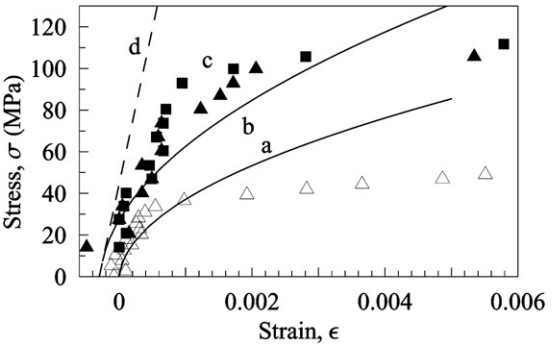

Figure 5. Tensile data is shown for (a) the 50 μm wire with $d = 14.7$ μm (open triangles), (b) the 10 μm wire with $d = 10.2$ μm (solid triangles) and (c) the 10 μm wire with $d = 9.7$ μm (solid squares). The elastic line is shown broken (d). The theoretical curves are calculated as described in the text. For (b) and (c), a single curve is given calculated for $d = 10$ μm and the origin is shifted to -0.0003 on the x-axis for better agreement with the data.

where b is the magnitude of the relevant component of the Burgers vector, $\bar{x}$ is the mean free path of mobile dislocations, some fraction of the grain size, $\bar{x} = \lambda d$, and ρ_m is the density of mobile dislocations, some fraction of the total density of dislocations, $\rho_m = \xi\rho$. The shear stress during plastic flow is determined by forest strain-hardening. It is given in terms of the total dislocation density ρ by

$$\sigma = \alpha b G \sqrt{\rho}, \tag{7}$$

where α is a coefficient, of the order of unity for forest strain-hardening. Eliminating ρ, the stress–strain relationship is

$$\sigma = \alpha G \sqrt{\frac{b\varepsilon_{pl}}{\lambda\xi d}}, \tag{8}$$

giving square-root strain-hardening and the Hall–Petch inverse square-root dependence of flow stress on grain size. In this form, the theory includes no other size effects: it explains only the Hall–Petch effect.

Equation (6), which is apparently a self-evident identity, deserves some discussion. The mean free path $\bar{x}$ and the Burgers vector b are clear; but the meaning of ρ_m is not. A differential expression $\mathrm{d}\varepsilon_{pl} = b\,\mathrm{d}(\bar{x}\rho_m)$ is more transparent. For the increment of plastic strain $\mathrm{d}\varepsilon_{pl}$, if $\bar{x}$ is constant, it is necessary for $\mathrm{d}\rho_m$ dislocations to move $\bar{x}$. For example, $\mathrm{d}\rho_m$ dislocations out of the existing density $\mathrm{d}\rho$ may become mobile or sources may operate to produce $\mathrm{d}\rho_m$ dislocations, requiring the creation of $\mathrm{d}\rho'$ dislocations such that $\mathrm{d}\rho_m = \xi\mathrm{d}\rho'$ but it does not follow that the total dislocation density ρ increases by $\mathrm{d}\rho'$. In small-volume plasticity, some or all of $\mathrm{d}\rho_m$ will exit the system instead of contributing to $\mathrm{d}\rho$. If most of them do, this is the phenomenon of dislocation starvation, as introduced by Greer and Nix [24] to explain the strength and strain-hardening behaviour of small pillars under compression. In this case, $\bar{x}$ is some fraction of the size of the structure, h, and $\mathrm{d}\rho < \mathrm{d}\rho'$. In general, we expect $\bar{x}$ to depend on some effective length $f(h, d)$.

When there is a plastic strain gradient, as in nanoindentation or in a wire in torsion, some dislocations running down the strain gradient will stop and will subsequently be described as geometrically necessary dislocations (GNDs). Part of $d\rho_m$ thus becomes $d\rho_{GND}$ and contributes to $d\rho$. This may reduce $\bar{x}$ more or less significantly ($\bar{x} < h$), but in any case ρ_{GND} may be calculated when ε_{pl} is known as a function of position. It seems unnecessary to introduce a characteristic length to parameterise their density, as is often done in strain-gradient plasticity theory (SGP) [3,4,25]. The present theory will subsume SGP quite naturally.

Thus, the general theory may be expressed as

$$\begin{aligned} d\varepsilon_{pl} &= b\,d(\bar{x}\rho_m) \quad \bar{x} = \lambda f(h,d) \\ d\rho &= \xi^{-1} d\rho_m \\ d\sigma &= \frac{1}{2}\alpha b G \frac{d\rho}{\sqrt{\rho}}. \end{aligned} \tag{9}$$

Conrad's theory as summarised in Equations (6)–(8) assumes that λ and ξ are constants, independent of ε_{pl}, and that $f(h,d) = d$ with $\bar{x} = \xi d$. We follow the first assumption since our fits to data have not required it to be abandoned. We do not follow the second assumption. In a finite structure, where the relevant structure size is h, the term for the average grain size d requires modification, i.e. we require an $f(h,d)$ which also involves h as well as d. The term for the average dislocation spacing $1/\sqrt{\rho}$ requires a corresponding modification which involves h and d as well as ρ. We showed in [15] and [22] that the relevant function to replace d is indeed $\ell_{eff} = f(h,d)$ given by Equation (1) if (and probably only if) grain boundaries and free surfaces act in the same way on mobile dislocations (i.e. remove them from the problem). By this, we mean that, just as a dislocation that arrives at a free surface is annihilated and ceases to contribute to the density ρ in Equation (9), similarly a dislocation arriving at a grain boundary is to cease to contribute to the density ρ in Equation (9). This may happen if, for example, mobile dislocations arriving at the same grain boundary from opposite sides annihilate or effectively cancel. We also showed in [22] that the term for the average dislocation separation in Equation (9), $\rho^{-1/2}$, should be decreased, becoming replaced by $(\rho^{\frac{1}{2}} + \ell_{eff}^{-1})^{-1}$. Both these modifications arise because a finite section of length h taken at random out of a distribution of points of density d^{-1} on an infinite line has an average separation given by the ℓ_{eff} of Equation (1). This was derived rigorously in [22] for Poisson distributions. It may be useful to picture the specimen, the wire, being cut out of bulk material with average grain size d and dislocation density ρ. The cutting out of the specimen of diameter a does not modify either d or ρ but it does preferentially select the smaller values from the distributions of d and $\rho^{-1/2}$. We refer to this coupling of h and d as 'Ehrler coupling'.

It is convenient to work only with strain, not stress. We define the elastic component of the total shear strain during plastic deformation, ε_{el}, as the flow stress σ divided by the shear modulus G. So we use a modified slip-distance theory, in which Equations (6)–(8) are modified to become

$$\begin{aligned} \varepsilon_{pl} &= b\bar{x}\rho_m = b\xi(h^{-1} + d^{-1})^{-1}\lambda\rho \\ \varepsilon_{el} &= \varepsilon_0 + \alpha b(\sqrt{\rho} + h^{-1} + d^{-1}) \\ \varepsilon_{pl} + \varepsilon_{el} &= \varepsilon. \end{aligned} \tag{10}$$

These three equations can be solved analytically for $\varepsilon_{pl}(\varepsilon)$, eliminating ρ and ε_{el}. The term ε_0 describes an intrinsic strength or elastic limit which includes, e.g. the Peierls stress. An initial dislocation density ρ_0 could also be included. It is interesting that, even when $\varepsilon_0 = 0$ and $\rho = 0$, the equations predict a non-zero yield strength or elastic limit, with $\varepsilon_{pl} = 0$ for $\varepsilon < \varepsilon_{elm}$ and:

$$\varepsilon_{pl} = \varepsilon - (\alpha b(\alpha - 2\lambda\xi) - \alpha(4b\xi\ell_{\text{eff}}\varepsilon + \alpha b^2(\alpha - 4\lambda\xi))^{1/2})/2\lambda\xi\ell_{\text{eff}}, \tag{10b}$$

where $\varepsilon_{elm} = \alpha b(h^{-1} + d^{-1})$.

In the form of Equation (10), with suitable handling of ξ and λ, the solution describes the Hall–Petch effect, the structure size effect, dislocation starvation and strain-gradient effects on both the elastic limit and on the strain-hardening. Because Equation (10) still treats plastic deformation as a local phenomenon with a pointwise-valid $\varepsilon_{pl}(\varepsilon)$ relationship, it does not account for the collective behaviour seen in small-scale plasticity, which can also be described as the space-limited source problem. For that, we need critical thickness theory (CTT). In [22], we showed that the geometrical approximation for CTT [26] is valid in the case of a wire under torsion. In the approximation, it is not sufficient for the maximum of an inhomogeneous stress distribution to exceed the yield strain, for plastic deformation to occur. It is necessary that the strain ε exceeds the yield strain ε_Y by an amount which depends on the size of the initial plastic volume. We form the excess strain-thickness product by taking the integral, $\int(\varepsilon(s) - \varepsilon_Y)\mathrm{d}s$ over the shortest dimension s of the strained volume (the thickness, in the case of epitaxial layers). Then, the condition for plastic deformation is that the excess strain-thickness product exceeds the magnitude b of the relevant component of the Burgers vector, for the extension of a single dislocation. The excess strain-thickness has to be greater still, by a multiple of b, for sources to operate within the strained volume and, hence, generate significant plastic strain; $4b$ for a spiral source [21] or $5b$ for a Frank–Read source [13]. This is the space-limited source problem – a dislocation source such as a Frank–Read source or a spiral source must be able to fit within the space available, with evident constraints on the radius of curvature of the dislocations constituting the source and, hence, on the stress that can drive the source. In the present problem, this means that it is not sufficient for the surface strain of the twisted wire to reach the yield strain. The strain κr must reach the yield strain at some radius within the wire $r_{ct} < a$ such that $\frac{1}{2}\kappa\ (a - r_{ct})^2 > b$ or $5b$, as appropriate. Then, this volume undergoes plastic deformation collectively. In the presence of a strain gradient, this effect may be largely responsible for the size effect at yield, due to the additional limitation on plastic volume that the strain gradient imposes, although it is unimportant at high plastic strain.

To fit the torsion data, it is convenient to calculate the unload angle, φ_U, as a function of the plastic strain. The torque, Q, under purely elastic strain on the twisted wire is

$$Q = G\int_{r=0}^{a} 2\pi r\,\kappa r\,r\,\mathrm{d}r = 2\pi\kappa G\frac{a^4}{4} = 2\pi G\frac{\varphi}{L}\frac{a^4}{4}, \tag{11}$$

where κ is the twist per unit length and the angle is $\varphi = \kappa L$ for wire of length L. When there is plastic strain $\varepsilon_{pl}(r)$, the torque becomes

$$Q = G\int_{r=0}^{a} 2\pi r\left(\frac{\varphi}{L}r - \varepsilon_{pl}(r)\right)r\mathrm{d}r = 2\pi G\frac{\varphi}{L}\frac{a^4}{4} - 2\pi G\int_{r=0}^{a} r^2\varepsilon_{pl}(r)\mathrm{d}r. \tag{12}$$

The unload angle φ_U is then given by

$$Q = 0 = 2\pi\frac{\varphi_U}{L}\frac{a^4}{4} - 2\pi\int_{r=0}^{a} r^2\varepsilon_{pl}(r)\mathrm{d}r \tag{13}$$

or

$$\varphi_U = \frac{4L}{a^4}\int_{r=0}^{a} r^2\varepsilon_{pl}(r)\mathrm{d}r. \tag{14}$$

To fit to the data, we use the full solution of Equation (10) for $\varepsilon_{pl}(\varepsilon)$, substituting $\varphi_L r L^{-1}$ for the total strain ε. The radius at which the elastic strain equals the elastic limit ε_{elm} that follows from Equation (10) is given by

$$r_{elm} = \frac{L}{\varphi_L}\varepsilon_{elm} = \frac{L}{\varphi_L}[\varepsilon_0 + \alpha b(a^{-1} + d^{-1})]. \tag{15}$$

For small values of φ_L, $r_{elm} > a$ and the deformation is purely elastic. Critical thickness theory is introduced by calculating the radius above which the excess strain-thickness product equals $5b$, given by

$$\int_{r=r_{ct}}^{a}\frac{\varphi_L}{L}(r - r_{ct})\mathrm{d}r = \frac{\varphi_L}{L}(a - r_{ct})^2 = 5b \;\Rightarrow\; r_{ct} = a - \sqrt{\frac{10bL}{\varphi_L}}. \tag{16}$$

For small φ_L, $r_{elm} > r_{ct}$ and no plastic deformation occurs. As φ_L is increased, r_{elm} decreases and r_{ct} increases. Dislocation sources start to operate when $\varphi_L = \varphi_{L0}$, such that $r_{elm} = r_{ct}$. According to critical thickness theory, the plastic deformation $\varepsilon_{pl}(\varepsilon, r)$ is then constant for r from r_{ct} to a [22]. Single axial dislocations are favoured under the same condition when b instead of $5b$ is used in Equation (16), defining φ_{LS}. Then, for $\varphi_L > \varphi_{L0}$ or $\varphi_L > \varphi_{LS}$ as appropriate:

$$\varphi_U(\varphi_L) = \frac{4L}{a^4}\left(\int_{r_{elm}}^{r_{ct}} r^2\varepsilon_{pl}(\varphi_L, r)\mathrm{d}r + \int_{r_{ct}}^{a} r^2\varepsilon_{pl}(\varphi_L, r_{ct})\mathrm{d}r\right), \tag{17}$$

where $\varepsilon_{pl}(\varphi_L, r)$ is given by the solution of $\varepsilon_{pl}(\varepsilon)$ of Equation (10) with $\varepsilon = \varphi_L r/L$. This integral can be evaluated analytically, but the analytic solution is much too lengthy to be useful. Putting numbers in, we therefore calculate the fits to data which are given in Figures 3 and 4. The magnitude of the Burgers vector of copper is taken to be 0.256 nm. In [22], we obtained an accurate fit only to the higher-strain data of Figure 4. Here, we start with the small plastic strain of Figure 3, which corresponds to less than one dislocation (the strain corresponding to a single axial screw dislocation along the whole length of the wire is indicated). We assume that dislocation sources are not yet in operation, so that b rather than $5b$ is appropriate. Only the largest grains will participate in this initial yielding and so we take the limit of $d = \infty$. Some small fraction only of the length of the wire will participate at first,

and we find that taking one-eighth gives a good fit to the data. This fraction of one-eighth is a fitting parameter that scales the fit vertically, without affecting either the yield-point or the shape of the curve. It is likely that h, the thickness of the plastic zone, is a function of φ_L, varying perhaps between $a - r_{ct}$ and a, but it is not clear how best to include this. Consequently, we assume that $h = \frac{1}{2}a$. Then, we get the fit to the data shown in Figure 1 with $d = \infty$, $\varepsilon_0 = 0.8 \times 10^{-4}$, $\alpha = 1$, and the product $\lambda\xi = 0.33$. This fit reproduces the yield points and the shapes of the curves excellently. Then, for the higher-strain data, simply putting d back to the measured average value dropping the factor of one-eighth and using $5b$, gives the fit of Figure 4. This fit is not identical to that of [22]; indeed, not quite as good, but as we commented there, it is unlikely that the fit is unique.

The fit to the tensile data is apparently much simpler, for in the absence of a strain gradient the stress–strain curve is just the solution of Equation (10). It is not necessary to include critical thickness theory, since the data are not good enough to resolve the elastic limit and the smallest resolved strain is much greater than the critical thickness contributions of b/h or $5b/h$. Then, we would expect to fit the tensile data with the same parameters except for $h = 2a$ instead of $\frac{1}{2}a$, since the dislocations can traverse the entire diameter of $2a$. Using the Tresca criterion (critical resolved shear stress) averaged over all possible grain orientations, the uniaxial yield stress may be taken to be a factor 3.1 greater than the yield stress in pure shear [27,28]. The data plotted in Figure 5 shows that the strength in tension is rightly estimated or perhaps slightly underestimated at the lowest strains. These strains are well into the plastic regime. The calculated elastic limits in tension are 4×10^{-5} for the 50 μm wire and $6–8 \times 10^{-5}$ for the 10 μm wires. So this data is to be compared with the data of Figure 4 in torsion. Then, at strains of 1×10^{-3} for the 50 μm wire and 2×10^{-3} for the two 10 μm wires, the strain-hardening rather abruptly stops and the wires become much weaker than the predictions at higher strain. This data is in good agreement with the tensile data reported by Fleck et al. [3] and Stölken and Evans [4]. We tentatively suggest that the idea of dislocation starvation [24] and the analysis of Lee et al. [29] for prestrained micropillars are relevant here. For example, it may be the case that, in the torsion experiments, the accumulation of the geometrically necessary dislocations with increasing strain requires new dislocation sources to operate with each increment in strain, while in the tension experiments, with no GNDs, "immortal sources" are eventually created after which there is little or no strain-hardening. It is interesting to note that the thicker wire initiates dislocation starvation (if this is the phenomenon) at a much lower stress; indeed, taking our data together with that of Lee et al. [29] suggests an inverse dependence on pillar or wire diameter. In any case, much better tensile data is required to resolve the details of the deformation in this region.

4. Discussion and conclusions

The behaviour of small structures in torsion appears to be the simplest to understand. Small pillars under compression and bulk specimens under nanoindentation are both subject to pop-in due to lack of dislocation sources in the small volume under study, and this leads to large scatter in the data and to strengths often

approaching theoretical strength. On the other hand, small pillars under compression and thin wires in tension are both subject to the effects of dislocation starvation in preventing strain-hardening [24,29]. In our torsion experiments, these distractions are not evident. Pop-in is not expected and is not observed. It seems likely that the strain gradient and the concomitant geometrically-necessary dislocations prevent dislocation starvation. There is no other evidence for the strain-gradient effects increasing the strain-hardening rate in torsion compared with tension. That is, strain gradient plasticity effects are important, controlling the rate of strain-hardening, but strain gradients are not *per se* responsible for the size effects.

When, as in these results, h and d couple as $(h^{-1} + d^{-1})^{-1}$, the Hall–Petch and the structure size effect must be due to a common physical mechanism. We suggest that the modified slip-distance theory used here accounts for both these phenomena. Moreover, the generalised slip-distance theory is expected to accommodate the ideas of dislocation starvation and strain gradient plasticity in a natural way. Further work is needed to see when and exactly how. Detailed comparison with discrete dislocation dynamics simulations, which can include grain boundaries [18], will be particularly valuable.

The role of strain gradients in this theory appears to be limited to controlling the boundary conditions that determine whether dislocation starvation occurs. However, a much better body of tensile data at low strains is needed. It is also expected that this theory can be applied – with the same parameters – to foil-bending and to nanoindentation; however, that is a matter for future work. The key result here is that the size effects in the elastic limit and in the strain-hardening of soft metals in torsion are both explained by the theory, with different mechanisms, but in both cases as a consequence of size alone. The physical origin of the size effect in the elastic limit is due to the constraint the size puts on dislocation curvature, while the physical origin of the size effect on the flow stress is due to the constraint size puts on dislocation mean free paths and on the boundary conditions that determine the fate of a dislocation after it has moved.

Acknowledgements

The late Professor Tony Evans brought the Conrad slip-distance theory to our attention when he was a Distinguished Visiting Professor at Queen Mary in 2007. Herr Bruno Ehrler explained the coupling of grain size and structure size in Equation (1) when he was an ERASMUS exchange student from Aachen University at Queen Mary in 2007. We acknowledge very useful discussions at the ECI Barga 2009 conference, particularly with Professor Bill Nix, Professor Bill Gerberich, Dr Nigel Jennett and Dr Karsten Durst. EPSRC provided financial support for this programme under grant EP/C518004/1.

References

[1] E.O. Hall, Proc. Phys. Soc. Lon. B 64 (1951) p.747.
[2] N.J. Petch, J. Iron Steel Inst. 174 (1953) p.25.
[3] N.A. Fleck, G.M. Muller, M.F. Ashby and J.W. Hutchinson, Acta Metall. Mater. 42 (1994) p.475.
[4] J.S. Stölken and A.G. Evans, Acta Mater. 46 (1998) p.5109.

[5] Q. Ma and D.R. Clark, J. Mater. Res. 10 (1995) p.853.
[6] T.T. Zhu, A.J. Bushby and D.J. Dunstan, J. Mech. Phys. Solids 56 (2008) p.1170; see also T.T. Zhu, A.J. Bushby and D.J. Dunstan, Mater. Tech. 23(2008) p.193 for a review.
[7] A.J. Bushby, T.T. Zhu and D.J. Dunstan, J. Mater. Res. 24 (2009) p.966.
[8] M.D. Uchic, D.M. Dimiduk, J.N. Florando and W.D. Nix, Science 305 (2004) p.986.
[9] C.A. Volkert and E.T. Lilleodden, Phil. Mag. 86 (2006) p.5567.
[10] F.C. Frank and J.H. van der Merwe, Proc. R. Soc. A 198 (1949) p.216.
[11] J.W. Matthews, Phil. Mag. 13 (1996) p.1207.
[12] E.A. Fitzgerald, Mater. Sci. Rep. 7 (1991) p.87.
[13] D.J. Dunstan, J. Mater. Sci. Mater. Electon. 8 (1997) p.337.
[14] X.D. Hou, A.J. Bushby and N.M. Jennett, J. Phys. D Appl. Phys. 41 (2008) p.074006.
[15] T.T. Zhu, B. Ehrler, X.D. Hou, K.M.Y. P'ng, A.J. Bushby and D.J. Dunstan. Available from: http://arxiv.org/abs/0910.5616.
[16] Y. Xiang, X. Chen and J.J. Vlassak, J. Mater. Res. 20 (2005) p.2360.
[17] B. Ehrler, X.D. Hou, T.T. Zhu, K.M.Y. P'ng, C.J. Walker, A.J. Bushby and D.J. Dunstan, Phil. Mag. 88 (2008) p.3043.
[18] A. Widjaja, E. Van der Giessen and A. Needleman, Acta Mater. 55 (2005) p.6408.
[19] C.R. Whitehouse, S.J. Barnett, B.F. Usher, A.G. Cullis, A.M. Keir, A.D. Johnson, G.F. Clark, B.K. Tanner, W. Spirkl, B. Lunn, W.E. Hagston and C. Hogg, Inst. Phys. Conf. Ser. 134 (1993) p.563.
[20] R.H. Dixon and P.J. Goodhew, J. Appl. Phys. 68 (1990) p.3163.
[21] R. Beanland, J. Appl. Phys. 72 (1992) p.4031; J. Appl. Phys. 77 (1995) p.6217.
[22] D.J. Dunstan, B. Ehrler, R. Bossis, S. Joly, K.M.Y. P'ng and A.J. Bushby, Phys. Rev. Lett. 103 (2009) p.155501.
[23] H. Conrad, S. Feuerstein and L. Rice, Mater. Sci. Eng. 2 (1967) p.157.
[24] J.R. Greer, W.C. Oliver and W.D. Nix, Acta Mater. 53 (2005) p.1821; J.R. Greer and W.D. Nix, Phys. Rev. 73 (2006) p.245410.
[25] W.D. Nix and H. Gao, J. Mech. Phys. Solids 46 (1998) p.411.
[26] D.J. Dunstan, S. Young and R.H. Dixon, J. Appl. Phys. 70 (1991) p.3038.
[27] G.J. Taylor, J. Inst. Metals 62 (1938) p.307.
[28] J.F.W. Bishop and R. Hill, Phil. Mag. 42 (1951) p.414 and p.1298.
[29] S.-W. Lee, S.M. Han and W.D. Nix, Acta Mater. 57 (2009) p.4404.